Maps of the Cosmos
ASP Conference Series, Vol. 216, 2005
M. Colless, L. Staveley-Smith, R. Stathakis

First Year WMAP Observations

C. L. Bennett[1]

Code 685, Goddard Space Flight Center, Greenbelt, MD 20771

Abstract. The results of the first year *WMAP* sky survey are full sky microwave maps in five frequency bands from 23 to 94 GHz. Calibration errors are $< 0.5\%$ and the low systematic error level is well specified. The cosmic microwave background (CMB) is separated from the foregrounds using the multifrequency data. The $2 \leq l \leq 900$ anisotropy power spectrum is cosmic variance limited for $l < 354$ with a signal-to-noise ratio >1 per mode to $l = 658$. The temperature-polarization cross-power spectrum reveals both acoustic features and a large angle correlation from reionization. The optical depth of reionization is $\tau = 0.17 \pm 0.04$. A best-fit cosmological model to the CMB and other measures of large scale structure works remarkably well with only a few parameters. The age of the best-fit universe is $t_0 = 13.7 \pm 0.2$ Gyr old. The matter density is $\Omega_m h^2 = 0.135^{+0.008}_{-0.009}$, the baryon density is $\Omega_b h^2 = 0.0224 \pm 0.0009$, and the total mass-energy of the universe is $\Omega_{tot} = 1.02 \pm 0.02$. For *WMAP* data alone, $n_s = 0.99 \pm 0.04$. The lack of CMB fluctuation power on the largest angular scales reported by *COBE* and confirmed by *WMAP* is intriguing. *WMAP* continues to operate, so results will improve.

1. Introduction

On February 11, 2003, the Microwave Anisotropy Probe space mission was renamed the Wilkinson Microwave Anisotropy Probe (WMAP), in honor of David T. Wilkinson of Princeton University, and the first scientific results of the mission were reported in 13 papers.

The central goal of the *WMAP* mission was to make full sky maps in five frequency bands while minimizing sources of systematic measurement errors. A CMB map is the most compact representation of CMB anisotropy without loss of information. The *WMAP* mission design is described by Bennet et al. (2003a) and the results are summarized by Bennett et al. (2003b).

The *WMAP* instrument was designed with a back-to-back optical system with 1.4 m × 1.6 m primary reflectors to provide for differential measurements of the sky. The primary and secondary reflectors direct radiation into two focal planes, with ten feed horns in each, as described by Page et al. (2003a,b) and Barnes et al. (2002). The feed horns are attached to orthomode transducers (OMTs) that split the polarization of the incoming signal into a differential correlation radiometer system with High Electron Mobility Transistor (HEMT) amplifiers (Jarosik et al. 2003a). There are ten "differencing assemblies": four W-band (~ 94 GHz), two V-band (~61 GHz), two Q-band (~ 41 GHz), one

[1]Charles.L.Bennett@NASA.gov

Ka-band ($\sim$ 33 GHz), and one K-band ($\sim$ 23 GHz). Precise frequencies for the radiometers are given by Jarosik et al. (2003). Undesirable $1/f$ noise is minimized by the design of the *WMAP* radiometers (Jarosik et al. 2003a). All radiometers have $1/f$ knees below 50 mHz; 18 of 20 are below 10 mHz; and 10 of the 20 are below 1 mHz.

The radiometers are passively cooled to $\sim$ 90 K with no mechanical refrigerators. In addition, no actively cycling heaters were permitted anywhere on the *WMAP* spacecraft. These design features helped to ensure a mechanically, thermally, and electronically quiet platform that minimizes the driving forces of systematic measurement errors.

WMAP scans large areas of the sky in short periods of time (Bennett et al. 2003) with a complex scan pattern that maintains the Observatory in a nearly constant survey mode of operations (except for only $\sim$ 1 hr for each of $\sim$ 4 station-keeping maneuvers per year). Approximately 30% of the sky is observed each hour. The Observatory spins at 0.464 rpm ($\sim$7.57 mHz) and precesses at 1 rev hr^{-1} ($\sim$ 0.3 mHz).

The 840 kg *WMAP* Observatory was launched aboard a Delta II 7425-10 rocket (Delta launch number 286) on 30 June 2001 at 3:46:46.183 EDT from Cape Canaveral. *WMAP* executed three phasing loops in the Earth-Moon system before a lunar-gravity-assist swing-by, a month after launch, catapulted *WMAP* to an orbit about the second Lagrange point of the Sun-Earth system, L_2. Station-keeping is performed approximately four times per year to maintain the Observatory in a Lissajous orbit about the L_2 point with the Earth-*WMAP* vector within about $\sim 1^\circ - 10^\circ$ of the Sun-Earth vector. Six months are required for L_2 to orbit half way around the Sun, allowing for full sky coverage. By 10 August 2001, *WMAP* was sufficiently stable in its L_2 orbit for CMB data-taking to commence. The first year observations, completed on 9 August 2002, correspond with a full orbit about the Sun, thus containing two sets of full sky observations.

2. Data Processing, Calibration, Systematic Errors, and Maps

All of the instrument data are down-linked to the ground without any on-board flight data processing, thus allowing full insight into potential systematic effects. Only a fraction of a percent of data was lost in the flow from the Observatory to the SMOC. About 1% of the received data were not used due to systematic error concerns (e.g., data taken during near station-keeping maneuvers). Of the $\sim$ 99% good data, the processing pipeline flagged observations where bright planets were in the beams so that these data would not used be used in making maps.

The heart of the data analysis efforts center on studies of systematic measurement errors (Hinshaw et al. 2003a). Components of spurious signals at the spin period are the most difficult to distinguish from true sky signals. The Observatory was designed to minimize all thermal and voltage variations and all susceptibilities to these variations, especially at the spin period, as discussed by Bennett et al. (2003a). In addition, high precision temperature monitors on the Observatory provide the data needed to verify that systematic errors from thermal variations are negligible. Jarosik et al. (2003b) report that in-

flight spin-synchronous effects from the radiometers are < 0.17 μK rms in the time-ordered-data (TOD), based on flight thermal variations multiplied by upper limits on component susceptibilities measured in ground testing. Analysis of flight data without use of characterizations derived from ground-based testing give < 0.14 μK rms from all sources (not just the radiometers). This is a factor of > 50 times smaller than the requirement that was set in the mission's systematic error budget. Thus, *no corrections to the first year WMAP data are required for spin-synchronous systematic errors.*

The core of the processing pipeline calibrates the data and converts the differential temperatures into maps. The data are calibrated based on the Earth-velocity modulation of the CMB dipole. A gain model of the radiometers was derived and fit by Jarosik et al. (2003b). Calibration is achieved within 0.5% accuracy, dominated by the statistical uncertainty in the absolute calibration.

Low levels of $1/f$ noise create stripes in the maps that affect the angular power spectrum and other statistics derived from the maps. A pre-whitening filter is applied to the TOD to minimize these artifacts. An estimate of the magnitude of the striping is given in Hinshaw et al. (2003a) for the maps, and by Hinshaw et al. (2003b) for the power spectrum.

The differential temperature data are formed into maps based on the technique introduced by Wright et al. (1996). *WMAP* observes the sky convolved with the beam pattern. This is equivalent to the spatial transform of the sky multiplied by the instrument's "window function." The beam patterns are measured in-flight from observations of Jupiter (Page et al. 2003b). Uncertainties in our knowledge of the beam pattern, although small, are a significant source of uncertainty for *WMAP* since they imply imperfect knowledge of the window function. A small difference between the A-side and B-side optical losses was derived based on dipole observations and corrected in the processing. Far sidelobes of the beam patterns, determined by ground measurements and in-flight using the Moon, have been carefully examined (Barnes et al. 2003). A small far-sidelobe correction is applied only to the K-band map.

We combine the radiometer results within each band to make the five full sky maps at effective CMB anisotropy frequencies 23, 33, 41, 61, and 94 GHz. Some of the more prominent features of the maps, including detected point sources, are described by Bennett et al. (2003b).

3. Foreground Analyses

The *WMAP* mission carries radiometers at five frequencies for the purpose of separating the CMB anisotropy from foreground emission based on their different spectra. The *WMAP* bands were selected to be near the frequency where the ratio of the CMB anisotropy to the contaminating foreground is at a maximum.

Bennett et al. (2003c) present a recipe for foreground masks based on K-band temperature levels. An extragalactic point source mask is also constructed based on selections from source catalogs. An additional 2% of pixels are masked due to these ~ 700 sources.

One technique for reducing the level of foreground contamination is to form a linear combination of the multifrequency *WMAP* data that retains unity response for only the emission component with a CMB spectrum. This technique

https://doi.org/10.1017/S0074180900196457 Published online by Cambridge University Press

was introduced for *COBE* by Bennett et al. (1992b) and applied to *WMAP* by Bennett et al. (2003c) to arrive at the internal (*WMAP* data only) linear combination map. The foregrounds are removed to a remarkable degree; however, the statistics of this internal linear combination map are complex and inappropriate for most CMB analyses. A maximum entropy method (MEM) approach is also used where pixel-by-pixel amplitudes are updated in accordance with the MEM residuals until low ($< 1\%$) residuals are achieved. The process results in a map of each emission component for each of the five *WMAP* bands. It shows the synchrotron spectrum steepening with increasing frequency, as would be expected for a spectral break due to synchrotron losses at ≈ 20 GHz. The spinning dust emission is limited to $< 5\%$ of the total Ka-band foreground.

For the CMB analyses we use a mask to exclude pixels where the Galactic emission is strong, combined with template fitting (using external data only) where the foregrounds can be adequately corrected. This approach does not complicate the noise properties of the maps. Bennett et al. (2003c) describe the template fitting in detail. The MEM results are used to assess the degree of foreground emission remaining after the template subtraction. The result is < 7 μK rms at Q-band and < 3 μK rms at both V-band and at W-band for $l < 15$. This remaining foreground emission constitutes $< 2\%$ of the CMB variance (up to $l = 200$) in Q-band, and $\lesssim 1\%$ of the CMB variance in V- and W-bands. Hinshaw et al. (2003b) demonstrate that this small residual foreground level has a negligible effect on the cosmological results.

A search was made for point sources in the *WMAP* data resulting in a catalog of 208 detected sources Bennett et al. (2003c). We include $\sim$700 sources in our mask, despite having only detected $\sim$200 sources at the 5σ level, because sources below this detection level still contribute an undesirable statistical contamination to the maps. Even beyond masking the 700 sources, we still need to make a statistical correction to the power spectrum for residual source contamination (Hinshaw et al. 2003b). The derived source counts give a power spectrum level of $C^{\rm src} = (15 \pm 3) \times 10^{-3}$ μK^{2}sr at Q-band. This is consistent with the level found in the bispectrum analysis of the maps (Komatsu et al. 2003) and the level found in fits to the map power spectra (Hinshaw et al. 2003b). The Sunyaev-Zeldovich Effect is barely detectable and is not a significant "contaminant" to the *WMAP* data.

4. Limits on Non-Gaussianity

Komatsu et al. (2003) search for non-Gaussianity in the *WMAP* CMB anisotropy maps using Minkowski functionals and a bispectrum estimator. It is widely believed that the CMB anisotropy arises from Gaussian linear fluctuations in the gravitational potential. The simplest expression for the overall primordial gravitational curvature perturbation, $\Phi(\mathbf{x})$, is a sum of a linear $\Phi_L(\mathbf{x})$ and weak nonlinear components: $\Phi(\mathbf{x}) = \Phi_L(\mathbf{x}) + f_{NL}[\Phi_L^2(\mathbf{x}) - \langle\Phi_L(\mathbf{x})\rangle^2]$ where Φ_L is the linear Gaussian portion of the curvature perturbation and f_{NL} is a nonlinear coupling constant. Then, $f_{NL} = 0$ corresponds to the purely linear Gaussian case. For the Minkowski functionals, Komatsu et al. (2003) find $f_{NL} < 139$ (95% CL) and for the bispectrum Komatsu et al. (2003) find $-58 < f_{NL} < 134$ (95%

https://doi.org/10.1017/S0074180900196457 Published online by Cambridge University Press

CL). The two consistent results demonstrate that the CMB anisotropy follows Gaussian statistics.

5. Multipoles

The *WMAP* -determined dipole is 3.346 ± 0.017 mK in the direction $(l,\ b)= (263.85° \pm 0.1°,\ 48.25° \pm 0.04°)$. The uncertainty of the dipole amplitude is limited by the *WMAP* 0.5% calibration uncertainty, which will improve with time.

The quadrupole is the $l = 2$ term of the spectrum $\Delta T_l^2 = l(l+1)C_l/2\pi$, i.e. $\Delta T_{l=2}^2 = (3/\pi)C_{l=2}$. Alternately, the quadrupole amplitude can be expressed as $Q_{rms} = \sqrt{(5/4\pi)\ C_{l=2}} = \sqrt{5/12}\ \Delta T_{l=2}$. The *WMAP* quadrupole, $Q_{rms} = 8 \pm 2\ \mu$K or $\Delta T_2^2 = 154 \pm 70\ \mu\text{K}^2$, is consistent with *COBE* but with tighter limits because of better measurements and understanding of foregrounds, which are still the leading uncertainty. The quadrupole value is low compared with values predicted by ΛCDM models that fit the rest of the power spectrum. ΛCDM models, in particular, tend to predict relatively high quadrupole values due to the enhanced, Λ-driven, integrated Sachs-Wolfe effect.

Hinshaw et al. (2003b) compute the angular power spectrum using 28 cross-correlations between the eight Q-, V-, and W-band differencing assemblies. The cross-power spectrum from the 28 pairs is considered in four l ranges. For $l \leq 100$ we use uniform pixel weighting of only V- and W-band data. This reduces the Galactic contamination where measurement errors are well below the cosmic variance. For $100 < l \leq 200$ we use uniform pixel weighting of the combined 28 pairs. For $200 < l \leq 450$ all 28 cross-power pairs are used with a transitional pixel weighting. The transitional pixel weighting, defined and discussed in detail in Appendix A of Hinshaw et al. (2003b), smoothly transitions the weighting from the uniform pixel weights in the signal-dominated $l < 200$ multipole regime to inverse-noise-variance weighting in the noise-dominated $l > 450$ multipole regime. For $l > 450$ all 28 pairs are used with inverse noise weighting. Our Monte Carlo simulations show that this approach is a nearly optimal scheme.

The angular power spectrum is shown for the *WMAP* data in Figure 1. The *WMAP* power spectrum agrees closely with *COBE* at the largest angular scales, and with CBI and ACBAR at the finer angular scales. We highlight the CBI and ACBAR results because they are a useful complement to *WMAP* at the smaller angular scales. The acoustic pattern is obvious. Page et al. (2003c) find that the first acoustic peak is $\Delta T_l = 74.7 \pm 0.5\ \mu$K at $l = 220.1 \pm 0.8$. The trough following this peak is $41.0 \pm 0.5\ \mu$K at $l = 411.7 \pm 3.5$ and the second peak is $48.8 \pm 0.9\ \mu$K at $l = 546 \pm 10$.

ΛCDM models predict enhanced large angle power due to the integrated Sachs-Wolfe effect. The *WMAP* and *COBE* data, on the other hand, have the opposite trend. The model is an excellent fit to the *WMAP* full power spectrum except, perhaps, at $l \lesssim 6$. Since only a small fraction of the total number of measured multipoles are involved, the statistical contribution of the $l \lesssim 6$ points to the overall power spectrum fit is small and does not greatly drive the overall best-fit model. *There is very little large scale CMB anisotropy power in our sky. This fact, first seen by COBE is confirmed by WMAP.*

https://doi.org/10.1017/S0074180900196457 Published online by Cambridge University Press

6. CMB Polarization and the Detection of Reionization

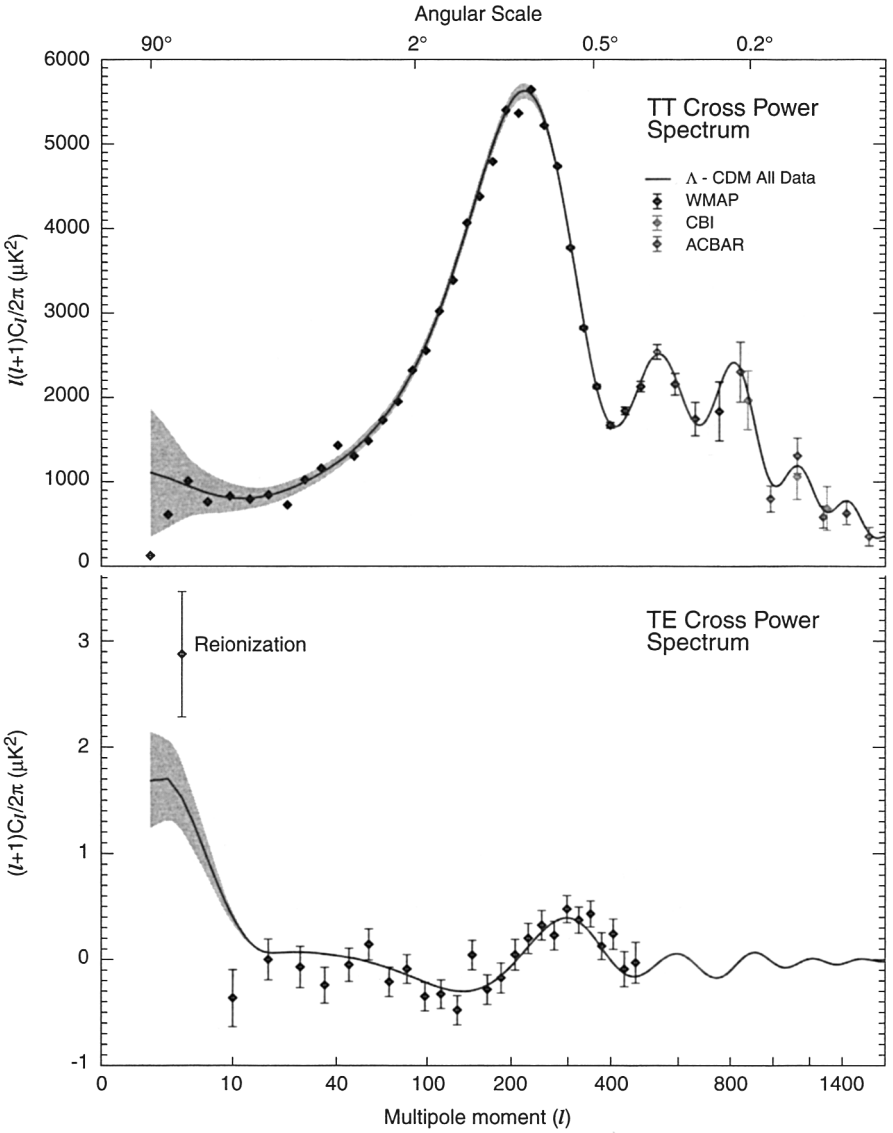

Figure 1. The *WMAP* angular power spectrum. (*top*:) The *WMAP* temperature (TT) results are consistent with the ACBAR and CBI measurements, as shown. The best fit ΛCDM model is shown with a grey band for the cosmic variance expected for that model. (*bottom*:) The temperature-polarization (TE) cross-power spectrum, $(l+1)C_l/2\pi$. (Note that this is *not* multiplied by the additional factor of l.) The peak in the TE spectrum near $l \sim 300$ is out of phase with the TT power.

https://doi.org/10.1017/S0074180900196457 Published online by Cambridge University Press

Kogut et al. (2003) report a detection of TE correlations on both large angular scales (from reionization) and on small scales (from the adiabatic fluctuations). The TE power spectrum, shown in Figure 1, is discussed in detail by Kogut et al. (2003). In the TE angular power spectrum the antipeak is $-35 \pm 9\ \mu\mathrm{K}^2$ at $l = 137 \pm 9$ and the peak is $105 \pm 18\ \mu\mathrm{K}^2$ at $l = 329 \pm 19$ (Page et al. 2003c).

The detection of the reionization of the universe corresponds to an optical depth $\tau = 0.17 \pm 0.04$ ($0.09 \leq \tau \leq 0.28$ at 95% confidence). Although *WMAP* measures the integrated optical depth, the epoch and redshift of reionization can be derived from the integral optical depth within the context of a model of the reionization process. For reasonable models, Kogut et al. (2003) conclude that the redshift of reionization is $z_r = 20^{+10}_{-9}$ (95% CL), corresponding to an epoch of reionization of $t_r = 180^{+220}_{-80}$ Myr (95% CL) after the Big Bang.

The measured optical depth means that reionization suppressed the acoustic peak amplitudes by $1 - e^{-2\tau} \approx 30\%$. While accounted for in our model fits, this suppression was not accounted for in previous CMB parameter determinations.

7. Cosmological Interpretation

The cosmological intepretation of first year results are discussed by Spergel et al. (2003), Peiris et al. (2003), Page et al. (2003c), and Kogut et al. (2003). The methodology used in the model fits is described by Verde et al. (2003). Spergel et al. (2003) show that a cosmological model with a flat universe, seeded with a scale-invariant spectrum of adiabatic Gaussian fluctuations, with reionization, is an acceptable fit not only to the *WMAP* data but also to a host of astronomical data. These data are: smaller angular scale CMB anisotropy data from ACBAR (Kuo et al. 2004) and CBI (Pearson et al. 2003); the HST key project value of H_0 (Freedman et al. 2001); the accelerating Universe seen in Type Ia SNe (Riess et al. 2001); the shape and amplitude of the large scale structure seen in clusters and superclusters of galaxies (Percival et al. 2001, Verde et al. 2003); and the linear matter power spectrum seen in the Lyman α forest (Croft et al. 2002). The optical depth since reionization is a new, but not surprising, component of the model. The *WMAP* data establishes this model as the standard model of cosmology by testing the key assumptions of the model and by enabling a precise determination of its parameters.

The *WMAP* data test several of the key tenets of the standard model. The *WMAP* detection of temperature-polarization correlations (Kogut et al. 2003) and the clear detection of acoustic peaks (Page et al. 2003c) implies that the primordial fluctuations were primarily adiabatic: the primordial ratio of dark matter/photons and the primordial ratio of baryons/photons do not vary spatially. The analysis of the *WMAP* temperature data demonstrates Gaussianity (Komatsu et al. 2003). The *WMAP* data, when combined with any one of the following three external data sets: HST Key Project measurement of H_0 (Freedman et al. 2001), the 2dFGRS measurement of the matter density (Percival et al. 2001, Verde et al. 2003) *or* the Type Ia supernova measurements (Riess et al. 2001) imply that the radius of curvature of the universe, $R = cH_0^{-1}|1-\Omega_{tot}|^{-1/2}$, must be very large, $\Omega_{tot} = 1.02 \pm 0.02$ and $0.99 < \Omega_{tot} < 1.05$ (95% CL). These measurements also require that the dark energy be the dominant constituent of

https://doi.org/10.1017/S0074180900196457 Published online by Cambridge University Press

Ω_{tot}. The *WMAP* data alone rule out the standard $\Omega_m = 1$ CDM model by $> 7\sigma$.

Our best fit model is a flat universe with a baryon fraction of $\Omega_b = 0.044 \pm 0.004$, a matter fraction of $\Omega_m = 0.27 \pm 0.04$, and a dark energy fraction of $\Omega_\Lambda = 0.73 \pm 0.04$, seeded with a scale-dependent spectrum of adiabatic Gaussian fluctuations. A combination of the *WMAP* data with the *COBE* determination of the CMB temperature (Mather et al. 1999), the CBI (Pearson et al. 2003) and the ACBAR (Kuo et al. 2004) CMB measurements, and the 2dFGRS survey determination of the power spectrum of the local galaxy fluctuations (Percival et al. 2001), yields the best fit cosmological parameters. Verde et al. (2003) describe our methodology for determining these parameters and Spergel et al. (2003) describe the best fit models for different combinations of data sets.

The *WMAP* detection of reionization at $z \sim 20$ is incompatible with the presence of significant warm dark matter density since the warm dark matter moves too fast to cluster in small objects at low z.

While the *WMAP* data alone are compatible with a wide range of possible properties for the dark energy, the combination of the *WMAP* data with either the HST key project measurement of H_0, the 2dFGRS measurements of the galaxy power spectrum *or* the Type Ia supernova measurements requires that the dark energy be 73% of the total density of the Universe, and that the equation of state of the dark energy satisfy $w < -0.78$ (95% CL).

WMAP's measurements of the baryon density, Hubble constant, and age of the universe strengthen the cosmic consistency that underlies the Big Bang model.

Atomic Density ($\Omega_b h^2$): Our best fit value is $\Omega_b h^2 = 0.0224 \pm 0.0009$. The baryon density is also probed via abundance measurements of [D]/[H]. It is impressive that $\Omega_b h^2$ is the same at $z = 1089$ as measured via the CMB as it is at $z = 10^9$ from Big Bang nucleosynthesis. Thus we find cosmic consistency of the baryon density throughout cosmic time and measurement technique.

Hubble Constant (H_0): The *WMAP* measurement of $H_0 = 71^{+4}_{-3}$ km s^{-1} Mpc^{-1} is remarkably consistent with the HST Key Project value of $H_0 = 72 \pm 3 \pm 7$ km s^{-1} Mpc^{-1} (Freedman et al. 2001). Through a variety of measurement techniques that sample different cosmic times and distances we find cosmic consistency on H_0.

Age of the Universe (t_0): The first acoustic peak in the CMB power spectrum represents a known acoustic size ($r_s = 147 \pm 2$ Mpc) at a known redshift ($z_{dec} = 1089 \pm 1$). From these, *WMAP* measures the age of the universe ($t_0 = 13.7 \pm 0.2$ Gyr) to an accuracy of $\sim 1\%$ by determining the CMB light travel time over the distance determined by the decoupling surface ($d_A = 14.0^{+0.2}_{-0.3}$ Gpc) and the geometry of the universe (i.e., flat). The age of the universe estimated via stars is consistent with age of the universe found by *WMAP*.

Matter Density ($\Omega_m h^2$): The matter density affects the height and shape of the acoustic peaks. The baryon-to-matter ratio determines the amplitude of the acoustic wave signal and the matter-to-radiation ratio determines the epoch, z_{eq}, when the energy density of matter equals the energy density of radiation.

https://doi.org/10.1017/S0074180900196457 Published online by Cambridge University Press

The amplitude of the early integrated Sachs-Wolfe effect signal is sensitive to the matter-radiation equality epoch. From these effects *WMAP* measures the matter density, $\Omega_m h^2$,to an accuracy of $\sim 5\%$. Large scale structure observations measure $\Omega_m h$ through the shape of the power spectrum. When combined with estimates of h, this yields $\Omega_m h^2$. Large scale velocity field measurements yield $\Omega_m^{0.6} b^{-1}$, where b is the bias in how the galaxy power spectrum traces the matter power spectrum ($P_{\rm gal} = b^2 P(k)$). Galaxy bispectrum measurements yield b, allowing for estimates of Ω_m. From the galaxy data, Verde et al. (2002) find $\Omega_m = 0.27 \pm 0.06$, which is consistent with the *WMAP* result of $\Omega_m = 0.27 \pm 0.04$.

WMAP results broadly support and constrain inflation models. Inflation predicts that the universe is flat. The combination of *WMAP* data with either H_0, Type Ia SNe, or large scale structure data constrains $|1 - \Omega_{tot}| < 0.03$. Inflation predicts Gaussian random phase fluctuations, consistent with *WMAP* data (Komatsu et al. 2003). Inflation predicts fluctuations on scales that appear to be superhorizon scales in a Friedman-Robertson-Walker (FRW) cosmology. The *WMAP* detection of an anti-correlation between polarization and temperature fluctuations on scales of $\sim 1^\circ - 2^\circ$ (Kogut et al. 2003) confirms this prediction and rules out subhorizon causal mechanisms for generating CMB fluctuations (Peiris et al. 2003). Inflation predicts a nearly scale invariant spectrum of fluctuations, as seen by *WMAP*. The *WMAP* data place significant constraints on r, the tensor-to-scalar ratio, n_s, the slope of the scalar fluctuations and $dn_s/d\ln k$, the scale dependence of these fluctuations. The addition of an admixture of isocurvature modes does not improve the *WMAP* model fits. The best fit model has a spectral index that runs from $n > 1$ on the large scales probed by *WMAP* to $n < 1$ on the small scales. The data, however, do not yet require $n > 1$ on large scales: our best fit model has $n_s = 1.03 \pm 0.04$ at $k = 0.002$ Mpc^{-1}.

8. Data Products

WMAP data are available through the Legacy Archive for Microwave Background Data Analysis (LAMBDA) at http://lambda.gsfc.nasa.gov. This is a new NASA data center dedicated to the rapidly growing field of microwave background data archiving and analysis. An Explanatory Supplement details the in-flight operations and data products (Limon et al. 2003). *WMAP* continues to collect data and is currently approved for 4 years of operations at L_2. The additional data, and more elaborate analyses, will help to further constrain models. The addition of other continuously improving CMB and large scale structure observations is essential for progress towards the ultimate goal of a complete understanding of the global properties of the universe.

Acknowledgments. I gratefully acknowledge the impressively talented and congenial WMAP Science Team. The *WMAP* mission is made possible by the support of the Office of Space Sciences at NASA Headquarters. I am also grateful to the National Radio Astronomy Observatory, which designed and produced the HEMT amplifiers that made *WMAP* possible.

References

Barnes, C., et al. 2002, ApJS, 143, 567
Barnes, C., et al. 2003, ApJS, 148, 51
Bennett, C. L., et al. 2003a, ApJ, 583, 1
Bennett, C. L., et al. 2003b, ApJS, 148, 1
Bennett, C. L., et al. 2003c, ApJS, 148, 97
Bennett, C. L., et al. 1992, ApJ, 396, L7
Croft, R. A. C., et al. 2002, ApJ, 581, 20
Freedman, W. L., et al. 2001, ApJ, 553, 47
Hinshaw, G. F., et al. 2003a, ApJS, 148, 135
Hinshaw, G. F., et al. 2003b, ApJS, 148, 63
Jarosik, N., et al. 2003a, ApJS, 145, 413
Jarosik, N., et al. 2003b, ApJS, 148, 29
Kogut, A., et al. 2003, ApJS, 148, 161
Komatsu, E., et al. 2003, ApJS, 148, 119
Kuo, C. L., et al. 2004, ApJ, 600, 32
Limon, M., et al. 2003, http://lambda.gsfc.nasa.gov
Mather, J. C., Fixsen, D. J., Shafer, R. A., Mosier, C., & Wilkinson, D. T. 1999, ApJ, 512, 511
Page, L., et al. 2003a, ApJ, 585, 566
Page, L., et al. 2003b, ApJS, 148, 39
Page, L., et al. 2003c, ApJS, 148, 233
Pearson, T. J., et al. 2003, ApJ, 591, 556
Peiris, H., et al. 2003, ApJS, 148, 213
Percival, W. J., et al. 2001, MNRAS, 327, 1297
Riess, A. G., et al. 2001, ApJ, 560, 49
Spergel, D. N., et al. 2003, ApJS, 148, 175
Verde, L., et al. 2002, MNRAS, 335, 432
Verde, L., et al. 2003, ApJS, 148, 195
Wright, E. L., Hinshaw, G., & Bennett, C. L. 1996, ApJ, 458, L53